16th World Conference on Earthquake, 16WCEE 2017
Santiago Chile, January 9th to 13th 2017
Paper N° 4637
Registration Code: S-T1461976361

Seismic risk assessment of wooden structures near faults considering the locational uncertainty of source area using the non-uniform slip model

M. Seikai[1], S. Nakahara[2], and M. Kohiyama[3]

[1] Graduate Student, Keio University, m_seikai@keio.jp
[2] Formerly Graduate Student, Keio University, s.nakahara926@gmail.com
[3] Professor, Keio University, kohiyama@sd.keio.ac.jp

Abstract

Although the magnitudes of inland earthquakes are smaller than those of earthquakes in subduction zones, they have caused catastrophic disasters in the past. Seismic damage to structures strongly depends on the geometric relationship between a fault and the structure itself, especially near a fault. In recent years, the locations and activities of inland active faults have been identified in Japan. However, the position of a rupture-starting point and rupture extent are uncertain. Together with this uncertainty, we have to consider the difference in the seismic performances of structures, upon which the extent of damage also depends. In this study, seismic ground motions near a fault were simulated with consideration of the above-mentioned uncertainty, and the geometric distribution of the damage probability of wooden structures near a fault was investigated. The effect of seismic performance was also investigated. First, the ground motion with directivity on an engineering bedrock was simulated with a non-uniform slip model of an earthquake-source fault using the stochastic Green's function. Element seismic waves overtook the phases of neighboring waves. Then, a rupture-starting point was decided stochastically and we assumed that the location of the earthquake-source fault followed a uniform distribution in the possible range. Ground motion on the surface was created by inputting the ground motion into a surface-layer model composed of loam using the one-dimensional equivalent linear analysis. If the maximum shear strain was over 5% in the response analysis result, we trimmed the input waves to maintain their reliability. Wooden structures were modeled considering the restoring force characteristics in accordance with the criteria of three seismic grades. Time-history response analysis was carried out by inputting the ground motion to the building model. Binomial discrimination as to whether or not damage occurred was conducted on the basis of the maximum story drift angle of the building models. Using the results of binomial discrimination, fragility curves assuming a lognormal distribution were constructed for each site using a maximum-likelihood method. Here the peak ground velocity was used as a ground-motion intensity parameter. A stochastic model of earthquake occurrence time was defined in consideration of the uncertainty of the earthquake scale, assuming a stochastic model for the variation of the slip quantity of the earthquake-source fault. We used a Brownian passage time distribution for making these models. Hazard curves of the ground motion were evaluated by this probability model. Finally, the earthquake damage probability of wooden structures was calculated for each site based on the fragility curve and the hazard curve mentioned above. As a result, the influence of the geometric relationship between a fault and the wooden structures and the seismic performance on the earthquake damage probability was obtained. The damage probability of wooden structures was significantly higher in the vicinity of the center of the possible range of the earthquake-source fault. In the vicinity of the fault, earthquake damage probability was reduced more effectively by changing the seismic grade from 1 to 2 than from 0 to 1.

Keywords: non-uniform slip model, risk assessment, seismic grade, uncertainty, wooden structures

1. Introduction

Active faults causing inland earthquakes exist in bedrock at depths of 15–20 km. Although the magnitudes of inland earthquakes are smaller than those of earthquakes in subduction zones, they have caused catastrophic disasters in the past, owing to severe local ground motion beneath living environments. In Japan, about 2,000 active faults capable of causing inland earthquakes have been identified.

Recently, various methods of predicting damage based on earthquake records and damage reports have been proposed and risk-evaluation results have been reported. The cabinet office of the government of Japan predicted and announced the seismic intensities of earthquakes that may occur in the future[1]. It is left to local governments to improve their disaster-reduction plans, but two problems remain. One is that the characteristics of ground motion differ depending on the positional relationship between a site and a fault; for example, the 1995 Kobe earthquake of M 7.3 caused critical damage to houses with a directivity pulse[2]. The other problem is that structural response varies according to structural characteristics such as height, structure type, and year of construction. Even ground motion of moderate amplitude can cause a high structure response owing to resonance. Differences in ground-motion characteristics appear strongly near earthquake faults.

Based on tectonic geomorphology and paleoseismological investigations, researchers have surveyed damage mechanisms by analyzing the characteristics of surface layers and the deformation and movement of the ground after earthquakes. Suzuki et al.[3] pointed out that although an active fault is supposed to slip massively, the slip distance could be one order of magnitude smaller than predicted and may happen more frequently. Such a smaller-sized earthquake occurred in Nagano Prefecture in 2014 and resulted in serious damage to houses. Therefore, even if a fault location has been identified and the scale of an earthquake due to the fault has been predicted, we should consider the uncertainty in the rupture areas of the faults and the scale of the earthquake to improve risk assessment.

This study first evaluates ground motions using an earthquake-source-fault model. Then, we calculate the damage-occurrence probabilities of wooden structures near the fault, considering differences in the seismic grade[4], which is a measure of seismic capacity based on the amount of bearing walls and braces. Finally, we clarify relations among earthquake damage risks to wooden structures, geometric position, and the earthquake resistances of structures.

2. Settings of the Fault Model

2.1 Setting the sites and the uncertainties of fault location and extent of rupture

In this study, we focus on sites near a fault. Figure 1 shows a possible range in which an earthquake-source fault can exist (blue areas) and a group of sites (green circles). We set the *x*- and *y*-axes and the origin point O, as shown in Fig. 1. The *x*-axis indicates the strike direction of a fault and the *y*-axis is set to be orthogonal to the *x*-axis. We set 98 sites that are arranged in lattice points. The top depth of the fault is assumed to be 0 km, the angle of inclination is assumed to be 90°, and the strike direction is assumed to be north. The earthquake-source-fault model is discretized every 1 km in the blue areas and we assume that fault location follows a uniform distribution, as shown in Fig. 2. Star marks in Fig. 2 represent possible rupture-starting points, explained in detail in Subsection 2.3.

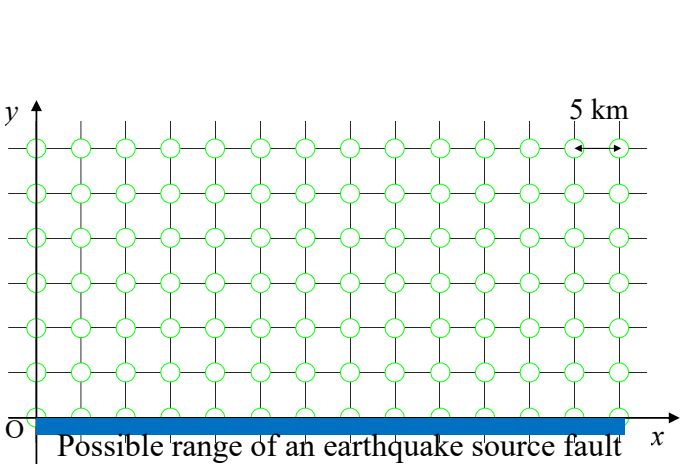

(a) Ground plan

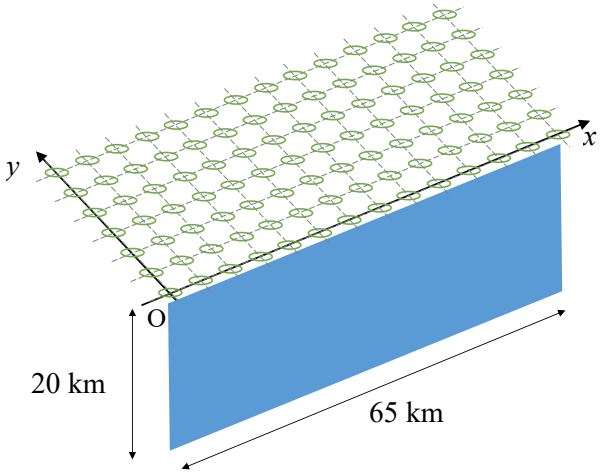

(b) Bird's eye view

Fig. 1 — Geometric positional relation between a fault and sites on the ground

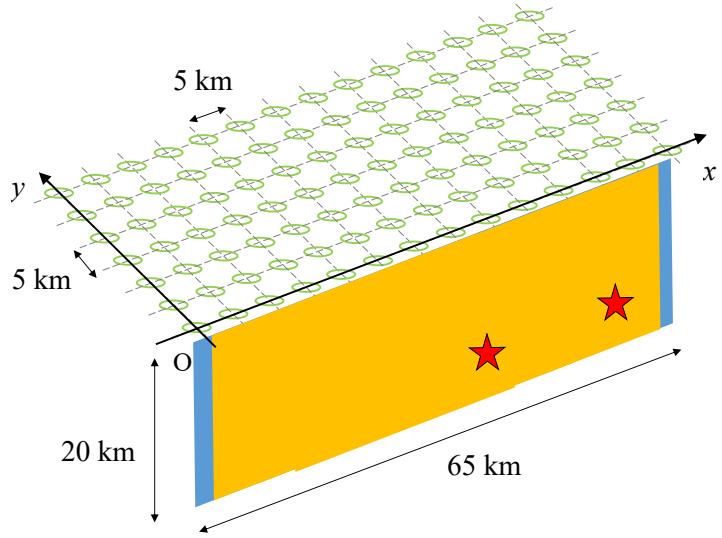

Fig. 2 — Possible locations of an earthquake-source fault (translucent yellow)

2.2 Uncertainty of the source-fault model and the rupture-starting point

Assuming an inland earthquake, we set parameters with reference to a "recipe" for strong ground-motion prediction[5]. We investigate 11 magnitude patterns from M 6.5 to 7.5. The width and length of a fault are determined based on the data obtained by Takemura[6] and Wells and Coppersmith (1994)[7], as shown in Table 1. The total area of asperities is 22% that of the fault[8]. We set one asperity for earthquakes with M 6.5–6.9 and two asperities for those with M 7.0–7.5[7]. When we assume two asperities, their area ratio is 2:1 according to Ishii et al.[9]. These asperities are placed near the center of the fault for simplicity.

Table 1 — Magnitude and size of faults

Magnitude	6.5	6.6	6.7	6.8	6.9	7	7.1	7.2	7.3	7.4	7.5
Width [km]	10	11	13	15	18	20	20	20	20	20	20
Length [km]	18	20	20	20	20	20	22	26	29	33	38

Somerville et al.[8] and Kikuchi and Yamanaka[10] revealed that rupture-starting points tend to exist at the corners of asperities. Moreover, in the case of inland strike-slip faults, the rupture proceeds from the deep part to the shallow. Hence, we set the rupture-starting points at the bottom corners of the asperities. Each corner is chosen with equal probability (hereinafter, the cases are called Cases 1 and 2) in Monte Carlo simulations. If two asperities exist, we set the starting point outside the asperities. For simplicity, we do not consider the scenario where rupture starts from the center. The source fault is divided into 1 km × 1 km square meshes, and each mesh is regarded as a small fault, which generates an element ground motion.

Figure 3 shows the cases with M 6.8 and M 7.4. The blue meshes represent the background areas of an earthquake-source fault, and the red meshes represent asperities. Stars indicate possible rupture-starting points.

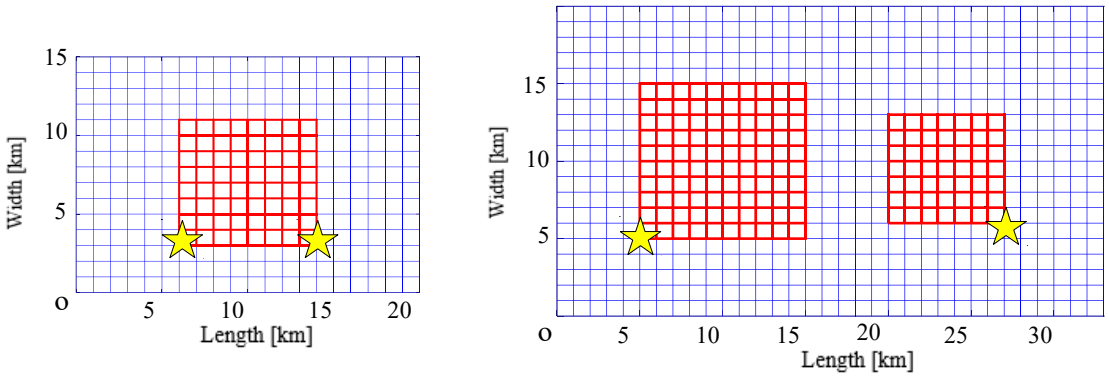

(a) M 6.8 (b) M 7.4

Fig. 3 – Examples of earthquake-source-fault models

3. Simulation of Earthquake Ground Motion Using a Stochastic Green's Function

3.1 Simulation of element waves

In this study, we use the stochastic Green's function[10] to simulate earthquake ground motion. First, we produce mutually independent white noises with a time interval, Δt, of 0.01 s (i.e., the effective frequency band ranges from 0 to 50 Hz) and a phase distributed uniformly from 0 to 2π for all fault elements. Second, we revise the phase characteristics of the white noise. In the case of sites near a fault, the directivity effect, which causes pulse-ground motion, must be presented. We assume that element waves have similar rupture processes on the fault and ground-propagation paths, and give coherent phases to the white noises used in the generation of element waves, as shown in Fig. 4. The procedure to modulate these phases is as follows:

Step 1: Generate white noises that are mutually independent.

Step 2: Give a randomly selected 25% of the frequency content of the element wave of fault 1 to the phases of the element wave of fault 2, and give random phases to the other 75% of the frequency content.

Step 3: Give a randomly selected 25% of the frequency content of the element wave of fault 1 to the phases of the element wave of fault 3, and give random phases to the other 75% of the frequency content.

Step 4: In fault 4, randomly select 25% of the frequency content to take on the phases of faults 2, another 25% to take on the phases of fault 3, and give random phases to the remaining 50%.

Next, we set up an envelope function and multiply it by the white noise in the time domain to obtain a model for an element waves. We adopt the envelope function of Ho and Kawase[12], which is a variant on that of Boore[13].

After that, the acceleration Fourier amplitude spectrum of the wave is modified by Boore's basis spectrum. Finally, element waves are converted into the time domain using an inverse-Fourier transform. These waves represent those on outcrop engineering bedrock.

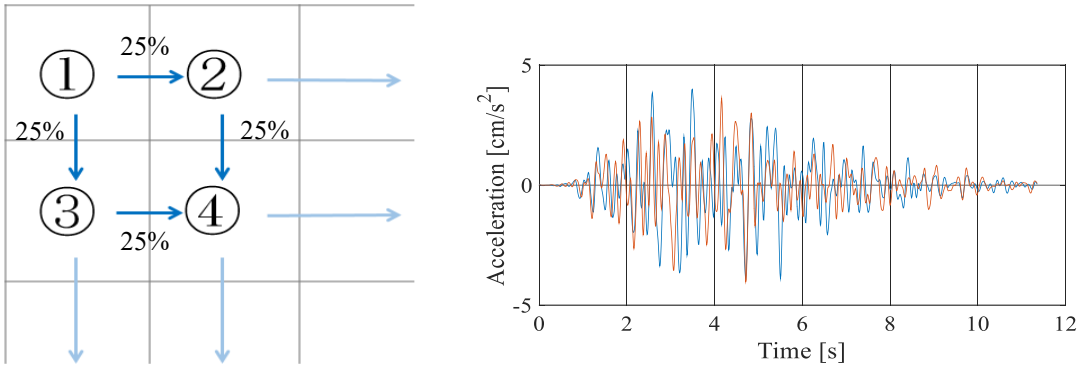

(a) Succession of phases (b) Element waves

Fig. 4 — Regulation of phases

3.2 Simulated earthquakes on the ground surface

We simulate earthquake ground motion using the waves explained in the previous subsection with DYNEQ, a computer program for one-dimensional equivalent linear analysis[14]. The subsurface ground at the site is assumed to be a loam layer with a depth of 20 m. The density and shear-wave velocity of the loam are 1.6 g/cm^3 and 200 m/s, respectively[14], [15].

After performing one-dimensional equivalent linear analysis, we check whether the maximum shear strain of the loam layer is not too large to offer a reliable analytical result. In this study, we adopt 5% of the maximum shear strain as our threshold; for values over 5%, we trim the input waves as described below based on the assumption that the maximum responses of houses occur at the time of the maximum amplitude of input waves and the wave part after the maximum amplitude, which increases the shear strain of the soil, is not important for judging the damage to the houses.

We assume that the excessive shear strain occurs after the acceleration amplitude reaches its maximum and that the shear strain remains within the effective range below 5% prior to this point. Based on this assumption, we try to find the time when the shear strain is less than 5%. We regard the input ground motion at the bedrock level as being effective until the first zero-crossing time after it reaches the maximum. After this point in time, the rest of the input ground-motion data is changed to 0 to conduct equivalent linear analysis.

Using the modified input ground motion, we perform equivalent linear analysis and check the maximum shear strain again. When we find that the strain is over 5%, we go back by 0.05 s to change the data to 0. We repeat this process until a shear strain of less than 5% is achieved. Figure 5 shows an example of the shear strain and simulated trimmed ground motion. The trimmed ground motion seems to be unrealistic; however, the maximum earthquake responses of wooden structures remain reliable because the maximum shear strain of the surface layer remains within a relatively small range.

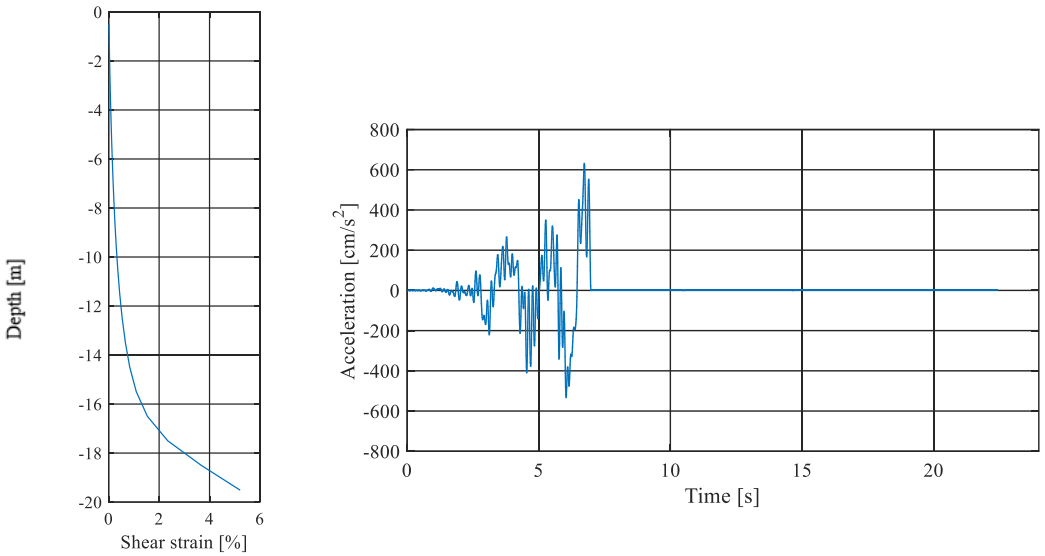

(a) Shear strain (b) Trimmed input wave

Fig. 5 — Example of a trimmed input wave (x = 15 km, y = 0 km, and M 7.2)

4. Fragility Evaluation of Wooden Structures

4.1 A wooden structure model

We consider a general two-story wooden building and construct a model using a two-mass shear-spring system. The details are shown in Fig. 6(a). The restoring force characteristics (Fig. 6(b)) are according to Isoda and Kawai[16] and are based on a spring formed by a combination of bilinear and slip springs. In this study, we deal with three types of seismic grades[4], 0, 1, and 2, as explained in Table 2.

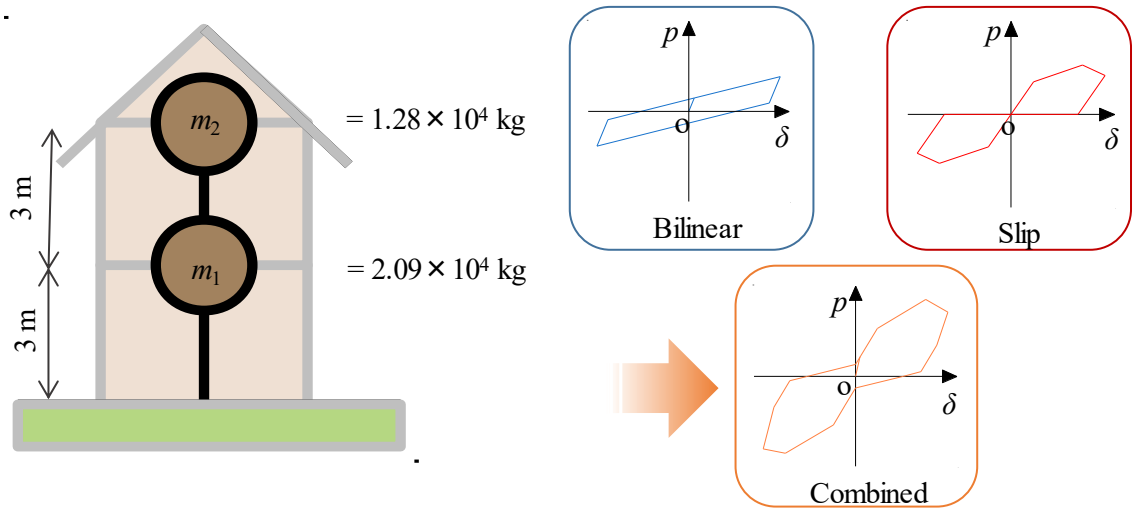

(a) Two-mass shear-spring system (b) Restoring force characteristics

Fig. 6 — A wooden structural model

Table 2 — Seismic grade[4]

Seismic grade	Explanation
0	A house of grade 0 does not meet the seismic standard in the enforcement ordinance with respect to the Building Standard Law.
1	A house of grade 1 can withstand a force generated by an extremely rare earthquake occurring approximately once every several hundred years without toppling or collapsing.
2	A house of grade 2 can withstand a force 1.25 times as strong as a force generated by an extremely rare earthquake occurring approximately once every several hundred years without toppling or collapsing.
3	A house of grade 3 can withstand a force 1.5 times as strong as a force generated by an extremely rare earthquake occurring approximately once every several hundred years without toppling or collapsing.

4.2 Damage evaluation and fragility curves

We calculate the maximum story drifts of wooden structure models using time-history analysis and judge whether the structures are damaged using a threshold of 1/60 rad[16], [17]; we assume that a maximum story drift over 1/60 rad indicates "damage." The scatter diagrams for making this judgment for three seismic grades are shown in Fig. 7. The maximum story drift in the large peak ground velocity (PGV) becomes smaller under higher seismic grades.

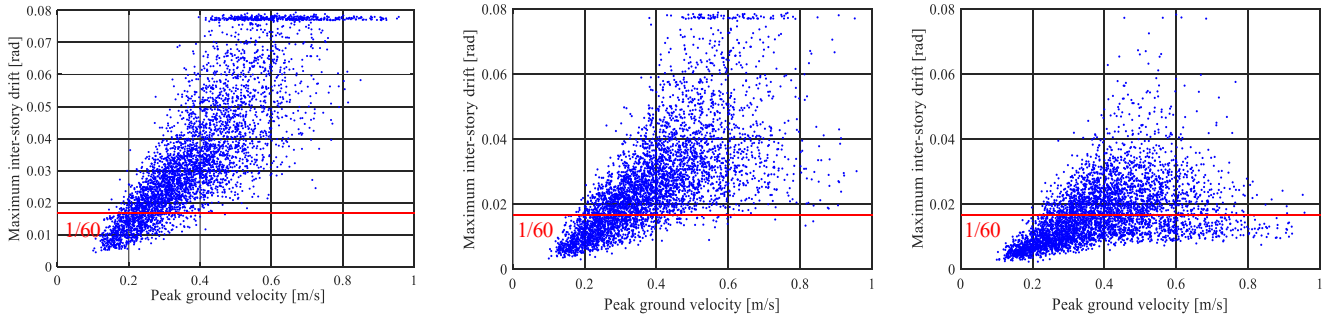

(a) Seismic grade 0 (b) Seismic grade 1 (c) Seismic grade 2

Fig. 7 — Scatter diagrams for damage determination (x = 30 km and y = 5 km)

Next, we evaluate the fragility curves at each site. The adopted ground-motion intensity parameter is the PGV, as in Okada and Takai[19]. These curves are approximated by a model using a lognormal distribution derived by the maximum-likelihood method. In this method, we use binary damage/no-damage data with a threshold of 1/60 rad. Figure 8 shows some samples of fragility curves. In Figure 8(c), the curve corresponding to y = 30 km has been omitted because we could not obtain sufficient samples showing damage in this case. The median (PGV at a damage probability of 50%) of these curves is small when the distance, y, from the x-axis is small. This means that even if sites have the same PGV, damage may differ due to differing periodic components in ground motions and damage is tend to occur near the earthquake-source-fault. Comparing the three graphs, the median is larger when the seismic grade is higher. Houses with higher seismic grades certainly reduce the probability of damage with their earthquake resistance.

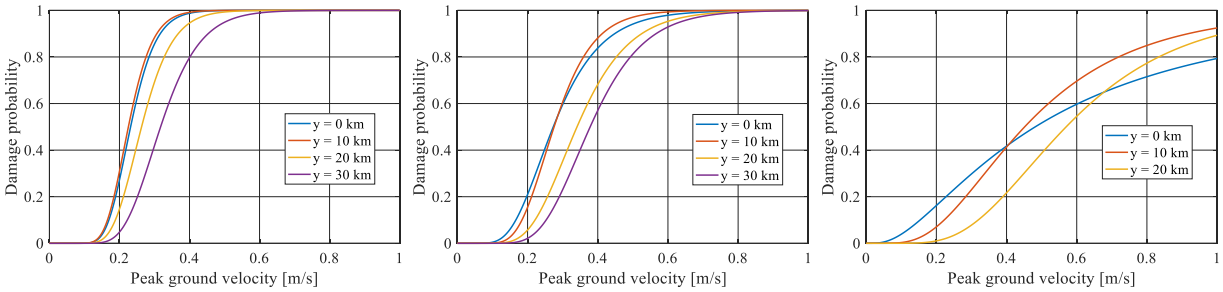

(a) Seismic grade 0 (b) Seismic grade 1 (c) Seismic grade 2

Fig. 8 — Examples of fragility curves (x = 30 km)

5. Damage probability evaluation

5.1 Uncertainty in earthquake magnitudes

The Headquarters for Earthquake Research Promotion have investigated the validity of the distribution model of earthquake occurrence intervals so as to improve the long-term evaluation of faults[20]. According to their investigations, a Brownian passage time (BPT) distribution is highly valid for presenting seismic activity intervals because its physical interpretation is easy to understand. Thus, we assume that the distribution of fault slip D (here we denote random variables in capital letters) follows a BPT distribution for which 0 years have passed since the latest seismic activity. Then, the probability density function, $f_D(d)$, of the fault slip D is given as follows:

$$f_D(d) = \left\{\frac{\mu_D}{2\pi\alpha^2 d^3}\right\}^{\frac{1}{2}} \exp\left\{-\frac{(d-\mu_D)^2}{2\mu_D\alpha^2 d}\right\}, \tag{1}$$

where μ_D is the average slip when an earthquake occurs and α is the variability of the activity intervals of a fault, which has a common value for each active fault. Based on the slip-prediction model, we consider the variability of the slip to be correlated with the variation in the number of years passed, and thus we use $\alpha = 0.24$, referring to the Headquarters for Earthquake Research Promotion[19].

The empirical formula for the fault slip d that occurs during an earthquake and its magnitude, M, is given on the basis of historic inland earthquakes in Japan as follows[21]:

$$\log d = 0.6M - 4.0; \tag{2}$$

thus, the probability density function of magnitude when an earthquake occurs is given by the following equation:

$$f_M(M) = f_D(10^{0.6M-4.0}). \tag{3}$$

Then, by discretizing and integrating Eq. (3), we obtain the following equation:

$$P[M = m] = \int_{M-\Delta M}^{M+\Delta M} f_M(m)\,\mathrm{d}m. \tag{4}$$

$P[M = m]$ means the probability that the magnitude, M, of an earthquake equals m, which is a discretized magnitude number. Figure 9 shows graphs of Eqs. (3) and (4).

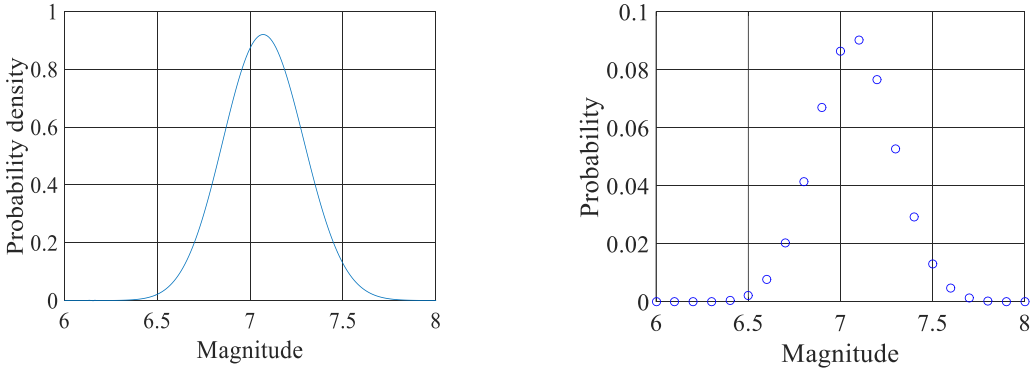

(a) Probability density function of Eq. (3) (b) Probability mass function of Eq. (4)

Fig. 9 — Probability density and mass functions of magnitude M

5.2 Evaluation of hazard curves

In this study, considering the general lifespan of wooden structures, we evaluate hazard curves with an evaluation period of t = 30 years for all target sites. We assume that the earthquake occurrence process follows the probability distribution of slip variability as we have explained before. The earthquake occurrence probability is calculated using the earthquake occurrence frequency over a year. We use PGV again as a ground-motion intensity parameter. The mean occurrence frequency in a year, $\lambda_i(v)$, of an event for which PGV exceeds the threshold v is expressed by Eq. (5) using Eq. (4):

$$\lambda_i(v) = N_0 \sum_m P[V \geq v \,|\, m] \cdot P[M = m], \tag{5}$$

where $P[V \geq v \,|\, m]$ is the probability that PGV equals or exceeds the threshold v when an earthquake with a magnitude of m occurs. Based on the set of synthesized ground motions of magnitude $M = m$, we model $P[V \geq v \,|\, m]$ using a logarithmic normal distribution. Note that we consider the hypocentral distance in the process of synthesizing ground motions. We approximate the PGV of the simulated ground motion using a logarithmic normal distribution model. N_0 is the number of earthquakes in a year with magnitudes larger than M_{min}, which can cause damage to structures, and we assign 0.1664 to N_0 with reference to J-SHIS[22]. From these preparations, we evaluate the probability, $P_h(v)$, using the following equation of a cumulative distribution function of an exponential distribution, which indicates that an earthquake for which the PGV is over v occurs at least once by time t:

$$P_h(v) = 1 - e^{-\lambda_i(v)t}. \tag{6}$$

The derived hazard curves are shown in Fig. 10. This proves that the shorter the distance y from the x-axis, the larger the PGV tends to be. Additionally, we can see from Fig. 10(b) that PGV tends to be smaller in sites with x-coordinates nearer to the center of the possible area of an earthquake-source fault.

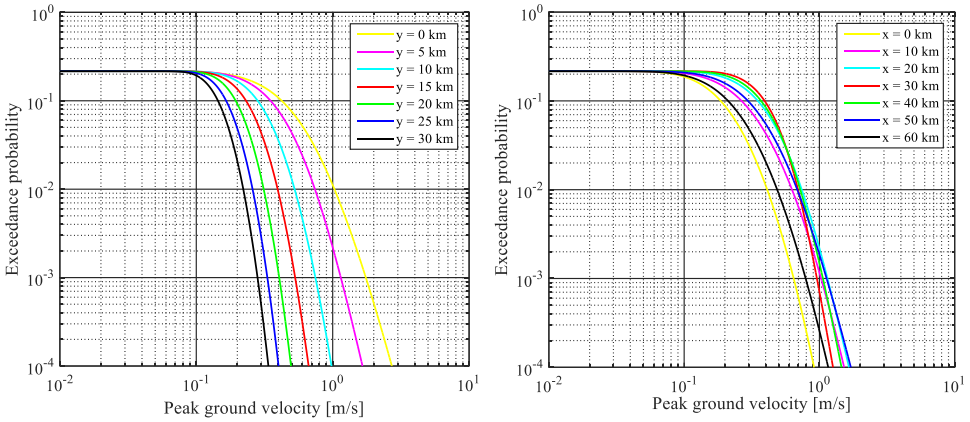

(a) $x = 20$ km (b) $y = 5$ km

Fig. 10 — Examples of hazard curves

5.3 Evaluation and distribution of damage probability

The damage probability of the wooden structures, P_d, is calculated by multiplying the probability density functions, $p_f(v)$, of the fragility curve, $P_f(v)$, and the hazard curve, $P_h(v)$, together and integrating the product from $v = 0$ to $v_{max} = 3$ m/s. Here, P_d is discretized by $\Delta v = 0.001$ m/s as in Eq. (7) and $p_f(v)$ is shown in Eq. (8):

$$P_d = \int_0^{v_{max}} p_f(v) P_h(v) \mathrm{d}v \approx \sum_{v=0}^{v_{max}} p_f(v) P_h(v) \Delta v \,, \tag{7}$$

$$P_f(v) = \frac{\mathrm{d}}{\mathrm{d}v} P_f(v) \,. \tag{8}$$

The damage probability distributions of wooden structures with seismic grades from 0 to 2 are shown in Fig. 11. The figure shows that the damage probability is larger at sites near the x-axis and around the center of the range of the earthquake-source fault. The reason for this is possibly that directivity pulse ground motions of both short and long periods tend to occur, and these motions can easily cause damage.

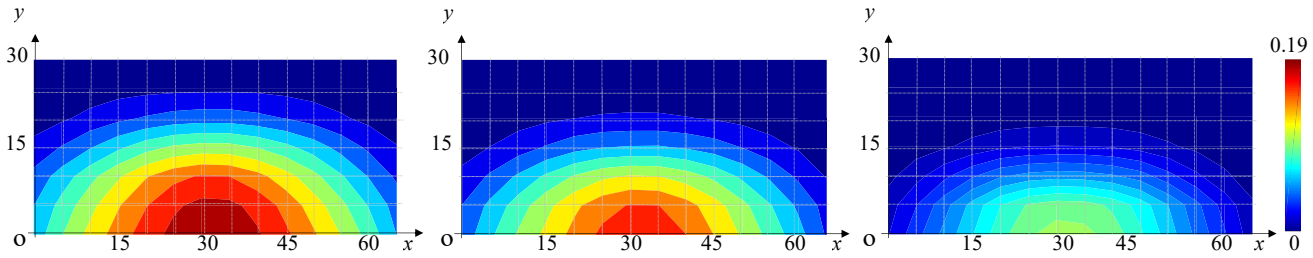

(a) Seismic grade 0 (b) Seismic grade 2 (c) Seismic grade 3

Fig. 11 — Damage probability over 30 years

5.4 Seismic strengthening effect

Finally, we examine the seismic strengthening effect in the site groups y = 0 km, 5 km, and 10 km, where seismic damage is relatively high. Here, the "risk ratio" represents the damage probability after strengthening divided by that before. We change the seismic grade from 0 to 1 or from 1 to 2. Figure 12 shows the relationship between sites and the risk ratio. The small value of the risk ratio means that the risk-reduction effect is greater, so we can say that it is more effective to change the seismic grade from 1 to 2 than from 0 to 1. This can be confirmed by the shapes of the fragility curves.

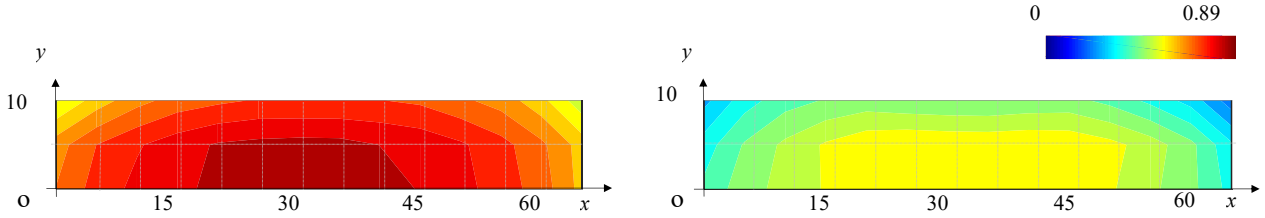

(a) Seismic grade from 0 to 1 (b) Seismic grade from 1 to 2

Fig. 12 — Relationship between sites and risk ratio

6. Conclusion

We evaluated the damage probabilities of wooden structures located around a strike-slip fault over 30 years. Ground motions are simulated using a non-uniform slip model considering uncertainty in fault location, earthquake magnitude, and the seismic performances of wooden structures. We observed that damage probability tends to be much higher near the center of the possible area of an earthquake-source fault and quantitatively showed that changing the seismic grade from 1 to 2 is more effective than changing it from 0 to 1. Future tasks include analyzing the similarities of adjacent fault elements and evaluating the case where different building models and different subsurface-ground models are used.

7. Acknowledgements

This research was financially supported by the Japan Society for Promotion of Science KAKENHI Grant-in-Aid for Scientific Research (B) 24360230 and 16H04455. In this study, the authors used improved computer programs, which was originally developed by Mr. Taku Watanabe, a former graduate student in Keio University.

References

[1] Headquarters for Earthquake Research Promotion (2014): *Zenkoku Jishindō Yosoku Chizu 2014 Nendo-ban—Zenkoku-no Jishindō Hazard-wo Gaikan-shite, Bessatsu: Shingen Dansō-wo Tokutei-shita Jishin-no Kyōshindō Yosoku Shuhō* (*Ground Motions Prediction Map in Japan, FY2014 edition—Overview of seismic hazard in Japan, Supplementary volume: A method for predicting strong ground motion for earthquakes with an identified earthquake source fault*, translated by the authors).

[2] Hisada Y (1998): Digitization of the Database for Direction of Collapsed Wooden Houses During the 1995 Hyogo-Ken-Nanbu Earthquake and Relations with Strong Motion Records. *Journal of Structural and Construction Engineering (Transactions of AIJ)*, 512, 105-110.

[3] Suzuki Y, Hirouchi D, Mitsuhisa W, Geomorphological Research Group for the 2014 Kamishiro Fault Earthquake (2015): Issues Raised by the 2014 Kamishiro Fault Earthquake, Central Japan. *Proc. General Meeting of the Association of Japanese Geographers, 2015 Spring General Meeting*, 1 p.

[4] The Building Center of Japan (2005): *The Housing Quality Assurance Act and Japan Housing Performance Indication Standards*. The Building Center of Japan

[5] Irikura K, Miyake H, Iwata T, Kamae K, Kawabe H, Dalguer LA (2004): Recipe for Predicting Strong Ground Motion from Future Large Earthquake. *Proc. the 13th World Conference on Earthquake Engineering*, CD-ROM, Paper No. 1371, 14 pp., Vancouver, British Columbia, Canada.

[6] Takemura M (1990): Scaling Low for Japanese Interplate Earthquakes in Special Relations to the Surface and the Damages. *Zisin (Journal of the Seismological Society of Japan, 2nd ser.)*, **2** (51), 211-228.

[7] Wells DL, Coppersmith KJ (1994): New empirical relationships among magnitude, rupture length, rupture width, rupture area, and surface displacement. *Bulletin of the Seismological Society of America*, **84** (4), 974-1002.

[8] Somerville P, Irikura K, Graves R, Sawada S, Wald D, Abrahamson N, Iwasaki Y, Kagawa T, Smith N, Kowada A (1999): Characterizing Crustal Earthquake Slip Models for the Prediction of Strong Ground Motion. *Seismological Research Letters*, **70** (1), 59-80.

[9] Ishii T, Sato T, Somerville PG (2000): Identification of Main Rupture Areas of Heterogeneous Fault Models for Strong-Motion Estimation. *Journal of Structural and Construction Engineering (Transactions of AIJ)*, 527, 61-70.

[10] Kikuchi M, Yamanaka Y (2001): Kiō Dai-jishin-no Hakai Katei = Asperity-no Dōtei (Rupture Process of the Past Large Earthquake = Identification of an Asperity, translated by the authors), *Seismo*, **5** (7), 6-7.

[11] Kamae K, Irikura K, Fukuchi Y (1991): Prediction of Strong Ground Motion Based on Scaling Law of Earthquake: By stochastic synthesis method. *Journal of Structural and Construction Engineering (Transactions of AIJ)*, 430, 1-9.

[12] Ho N, Kawase H (2007): Broadband Stochastic Green's Functions Based On Observed Data by Strong Motion Networks and Its Application to Nankai earthquake. *Journal of Japan Association for Earthquake Engineering,* **7** (2), 80-95.

[13] Boore DM (1983): Stochastic Simulation of High-Frequency Ground Motions Based on Seismological Models of the Radiated Spectra. *Bulletin of the Seismological Society of America*, **73** (6), 1865-1894.

[14] Yoshida N, Suetomi I (1996): DYNEQ: Tōka Senkei-hō-ni Motozuku Suihei Seisō Jiban-no Jishin Ōto Kaiseki Program (Seismic response analysis program for horizontally layered ground based on linear equivalent analysis, translated by the authors), *Reports of Satokogyo Engineering Research Institute*, 22, 61-70.

[15] Koyamada K, Miyamoto Y, Miura K (2003): Nonlinear Property for Surface Strata from Natural Soil Samples. *Proc. 38th Japan National Conference on Geotechnical Engineering*, 2007-2008.

[16] Isoda H, Kawai N (2007): Hysteresis Model of Walls on Japanese Conventional Construction: Study on seismic behavior of wooden construction. *Journal of Structural and Construction Engineering (Transactions of AIJ)*, 616, 157-163.

[17] Yoshida S, Ooi M, Mamoru Mizutani, Tanouchi K, Imazuka Y, Fujiwara H (2003): Study on Seismic Fragilities of Categorized Wooden Houses: Part 2: Study based on Monte Carlo simulation. *Summaries of Technical Papers of Annual Meeting Architectural Institute of Japan.* **B-2***,* 51-52.

[18] Tsuchimoto T, Ando N, Arima T, Nakajima S, Okazaki Y, Nakamura N (1998): A Clarification of Collapse Modes and an Establishment of Evaluation Methods of Earthquake Resistant Properties on Wooden Houses. *Annual of Housing Research Foundation,* 25, 259-270.

[19] Okada S, Takai N (2004): Damage Index Function of Wooden Structures for Seismic Risk Management: Proposal of the methodology based on deterministic approach. *Journal of Structural and Construction Engineering (Transactions of AIJ),* 582, 31-38.

[20] Headquarters for Earthquake Research Promotion (2001): *Chōki-teki-na Jishin Hassei Kakuritsu-no Hyōka Hōhō-ni-tsuite* (*About the method for long-term evaluation of seismic occurrence probability*, translated by the authors), http://www.jishin.go.jp/main/choukihyoka/01b/chouki020326.pdf (as of April 14, 2016).

[21] Matsuda T (1975): Magnitude and Recurrence Interval of Earthquakes from a Fault. *Zisin (Journal of the Seismological Society of Japan, 2nd ser.)*, **28**(3), 269-283.

[22] National Research Institute for Earth Science and Disaster Resilience: *Japan Seismic Hazard Information Station (J-SHIS)*, http://j-shis.bosai.go.jp/ (as of April 14, 2016).